COF Shell Microspheres

Deutsche Ausgabe: DOI: 10.1002/ange.201606155
Internationale Ausgabe: DOI: 10.1002/anie.201606155

Manipulation of Amorphous-to-Crystalline Transformation: Towards the Construction of Covalent Organic Framework Hybrid Microspheres with NIR Photothermal Conversion Ability

Jing Tan, Supawadee Namuangruk, Weifu Kong, Nawee Kungwan, Jia Guo, and Changchun Wang*

Abstract: *An approach to transforming amorphous organic networks into crystalline covalent organic frameworks (COFs) with retention of the colloidal nanosize and uniform morphology is presented. Specifically, Fe_3O_4 nanoclusters are encapsulated by a disordering polyimine network via the Schiff-base reaction. The formed imine bonds could be reconstructed under thermodynamic control to reform the polyimine networks into imine-linked COFs in situ. Such a core–shell microsphere exhibits the uniform size and spherical shape, controllable COF shell thickness, accessible surface modification, and improved solution dispersibility as well as maintenance of high surface area, periodic micropores, and superior magnetic responsiveness. Additionally, the photothermal conversion effect is demonstrated for the first time on the nanoCOF layers upon exposure to near infrared light, providing convincing evidence for potential use in phototherapy.*

Covalent organic frameworks (COFs) are two- or three-dimensional crystalline porous polymers that originate from the topological polymerization of building blocks with predesigned geometry and symmetry by virtue of dynamic covalent bonds (e.g. imine,[1] enamine,[2] hydrazine,[3] azine,[4] β-ketoenamine,[5] and boronate ester[6]). This emerging family presents high and regular porosity, tunable pore size and pore wall chemistry, and structural predictability and stability.[7] These characteristics endow COFs with outstanding performances for a wide-range of applications, such as gas storage,[8] heterogeneous catalysis,[9] luminescence,[10] optical sensing,[11] proton conduction,[12] and photoconduction.[13] Against this backdrop, there has been significant interest very recently in the miniaturization of COFs to the nanometer scale,[14] for the sake of extending the applicability and enhancing the properties of COFs. Indeed, the nanoCOFs can overcome, to some extent, the poor solution properties of the corresponding bulk materials, and they have been developed into nanocarriers for biomedical applications, such as drug delivery[15] and enzyme immobilization.[14b] However, most of the materials described were not very compatible with biomedical and pharmaceutical applications, and, with few exceptions, they were not engineered as dispersible nanoparticles to enable in vivo circulation by intravenous administration. As far as is known, the COF assemblies are prepared with no way of controlling size and morphology under solvothermal conditions. It is often seen that different morphologies and grain sizes are mixed and very difficult to isolate from each other. The early studies have demonstrated that the modulation of molecular conformation[14a,c] or assembly evolution via the Ostwald ripening process[14b] could create the hollow spherical nanoCOFs, but either the structural regularity is ill-defined or the formed particle body is short of uniformity both in terms of size and shape. Therefore, controlled synthesis of high-quality nanoCOFs remains largely challenged. In the context, motivated by the self-healing ability of dynamic covalent bonds, we imagined a scenario of disorder-to-order transition from amorphous organic networks to crystalline COFs, unlike the traditional bottom-up synthesis that requires the starting from building blocks. It is more feasible than directly modulating the colloidal properties of the nanoCOF during its growth.

Photothermal therapy, which employs photosensitizers to generate heat from light absorption giving rise to photoablation of cancer cells and subsequent cell death, has been shown to be a promising technique in cancer therapeutics.[16] Materials currently under investigation with efficient photothermal conversion mainly include metal plasmonic nanostructures, semiconductor nanoparticles, ferromagnetic nanoparticles, and conjugated polymers.[17] Beyond that, graphene is also a promising photothermal agent that possesses a high absorption intensity in the near-infrared (NIR) region and excellent heat generation efficiency.[18] COFs with distinct two-dimensional atomic structure could be comparable to graphene in some sense, because of their similarity in structure. Also, COFs allow for the rapid dissipation of generated heat to the surroundings by circulating the heat-transfer medium through the opening pore channels, which is distinct from the closed-cell porous systems restricting heat flow for thermal resistance.[19] We recently demonstrated that the open structure of conjugated microporous polymers facilitate heat conduction in water for a quick change of

[*] J. Tan, W. Kong, Prof. Dr. J. Guo, Prof. Dr. C. Wang
State Key Laboratory of Molecular Engineering of Polymers, Department of Macromolecular Science and Lab of Advanced Materials
Fudan University
220 Handan Road, Shanghai 200433 (China)
E-mail: guojia@fudan.edu.cn
Dr. S. Namuangruk
National Nanotechnology Center (NANOTEC), National Science and Technology Development Agency
Pathumthani 12120 (Thailand)
Prof. Dr. N. Kungwan
Department of Chemistry, Faculty of Science, Chiang Mai University
Chiang Mai 50200 (Thailand)

Supporting information for this article can be found under: http://dx.doi.org/10.1002/anie.201606155.

system temperatures.[20] As such, it could be anticipated that the use of COFs is a novel and attractive pathway toward the development of organic photothermal agents. To our knowledge, this is the first time that the potential of nanoCOFs for phototherapy has been evaluated.

To achieve this goal, we applied a template-mediated precipitation polymerization on an Fe_3O_4 nanocluster to give a core–shell microsphere containing an Fe_3O_4 nanocluster core and an amorphous polyimine network as the shell. We then performed the disorder-to-order reformation under solvothermal control to re-organize the polyimine network into the imine-linked COF as the shell. As shown in Scheme 1,

Scheme 1. The preparation of imine-linked COF composite microspheres through the amorphous-to-crystalline conversion process.

citrate-stabilized Fe_3O_4 nanoclusters were solvothermally synthesized according to a reported method.[21] Abundant carboxylate groups on the particle surface not only offer the dispersion stability in solution, but also help initiate the coverage by the polyimine network due to the H-bonding interaction, by which the monomer benzidine (BD) was preferentially anchored to the template particles. Then the polyimine network shell was created through the template-controlled precipitation polymerization of BD and 1,3,5-triformylphloroglucinol (Tp) in THF by the Schiff-base reaction. The obtained polymers were amorphous in texture but had the intrinsic imine linkage, which could be subjected to a dynamic covalent chemistry under conditions of equilibrium control achieving a structural transformation from disorder to order. Very recently, Dichtel et al. investigated the growth kinetics of imine-linked COFs, which showed the significant difference with boronate ester COFs that were formed during the simultaneous polymerization and crystallization.[22] The evolution of imine-COFs involved the rapid initial formation of amorphous networks and then gradual crystallization for the 2D topological structure. In light of the two-stage growth of imine-COFs, we employed the typical solvothermal method to rearrange the shell network structure of the Fe_3O_4@Polyimine microspheres in the mixed solvent of *n*-BuOH and *o*-dichlorobenzene (1:9 vol/vol). Pyrrolidine was used as the catalyst and the reaction proceeded at 120 °C for 3 days in a sealed and degassed Pyrex tube. High-resolution transmission electron microscope (HR-TEM) images displayed the size and shape of the products (Figure 1 a–c). It can be seen that after the initial polymerization, the polyimine network deposited on the Fe_3O_4 particles, forming a 100 nm thick organic shell with continuous and smooth appearance (Figure 1 b). Upon exposure to the conditions that facilitated the imine exchange, the reformed shell seemed to be assembled by many grains, while had almost the same thickness (Figure 1 c). Both before and after the solvothermal treatment, the microspheres evidently exhibited the well-defined core–shell structure, the narrowly

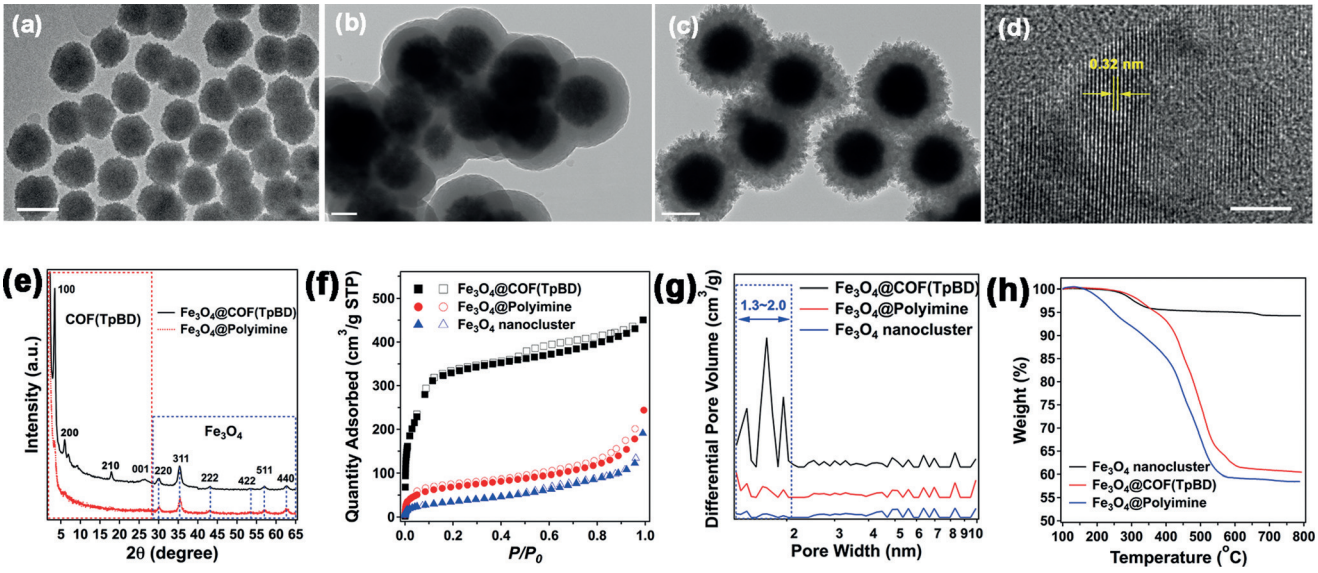

Figure 1. a–d) HR-TEM images of Fe_3O_4 nanoclusters (a), Fe_3O_4@Polyimine (b), Fe_3O_4@COF(TpBD) (c), and expanded view of the crystalline area (d). e) PXRD patterns of Fe_3O_4@Polyimine and Fe_3O_4@COF(TpBD). f–h) N_2 adsorption–desorption isotherms (f), pore size distributions (g), and TGA curves (h) of Fe_3O_4 nanoclusters, Fe_3O_4@Polyimine, and Fe_3O_4@COF(TpBD). The scale bars in a)–c) are 200 nm and in d) 5 nm.

distributed particle size, and the uniform spherical shape, without observation of any impurities. Mappings of Fe, O, C, and N atoms showed the distribution strictly according to the form of core–shell structure (see Figure S1 in the Supporting Information). Then the view on the edge of the COF shell was expanded to examine the ordering of molecular alignment. Figure 1 d shows the representative crystalline domain, arising from the stacking of parallel 2D sheets with an average separation of 0.32 nm, again, which had been determined by the selected area diffraction (Figure S2). Characterization of the microspheres by FT-IR spectroscopy provided evidence for the imine formation through the condensation of amine and aldehyde groups and the successive interconversion from enol to keto forms on the frameworks (Figure S3).[2,23]

PXRD patterns of Fe_3O_4@COF(TpBD) microspheres (Figure 1 e and Figure S4 for a larger view) showed the most intense peak at 3.4° corresponding to the (100) reflection plane, with the other diffraction peaks at 6.0°, 17.9°, and 26.4° assignable to the (200), (210), and (001) reflection planes as same as the reported data,[2b] and at 30.0°, 35.3°, 43.1°, 53.3°, 57.0°, and 62.6°, which were indexed to the cubic structure of Fe_3O_4 crystals, according to JCPDS 75-1610. In contrast, Fe_3O_4@Polyimine microspheres had only a very weak shoulder at about 3.4°, implying that the polyimine network is amorphous in nature.

To evaluate the porous structure, N_2 sorption measurements were carried out at 77 K. For the Fe_3O_4@COF(TpBD) microspheres, the isotherm sorption profiles were observed with the typical type I characteristics. In accordance with the IUPAC classifications, it is indicative of a micropore character (Figure 1 f). The Brunauer–Emmett–Teller (BET) surface area and pore volume were calculated to be as high as 1346 $m^2 g^{-1}$ and 0.25 $cm^3 g^{-1}$, respectively. Because of the loose compact and rough texture in Fe_3O_4 and Fe_3O_4@Polyimine, they showed a certain of BET surface areas, that is, 255 $m^2 g^{-1}$ for Fe_3O_4@Polyimine and 123 $m^2 g^{-1}$ for Fe_3O_4, but both were far less than that of the COF-based microspheres. The pore size distributions of the three samples were calculated by the nonlocal density functional theory method (Figure 1 g). Fe_3O_4@COF(TpBD) had the pore size predominated from 1.3 to 2.0 nm, which also agreed with the bulk COF-(TpBD).[2b]

Thermogravimetric analysis (TGA) revealed the thermal stability and mass ratios of different components (Figure 1 h). For the Fe_3O_4@Polyimine and Fe_3O_4@COF(TpBD) microspheres, they had the almost similar weight losses of 42 wt% and 40 wt%, respectively. It implies that the amorphous-to-crystalline conversion is high yielding, and the crystallization might proceed in a step-by-step manner without destruction of the whole shell. According to the residual weight, the loading content of COF-(TpBD) in the microspheres was estimated to be 36 wt%.

To our knowledge, acetic acid aqueous solution is the only catalyst used for the synthesis of imine-linked COF because the imine formation often requires acidic activation of the carbonyl compound and/or irreversible water removal. However, in our case, the acidic catalysts severely affected the formation of core–shell structures in the process of disorder-to-order transformation. It was observed that the Fe_3O_4 core was partially etched by acid over 3 days (Figure S5), although the crystallization occurred on the polymer shells (Figure S6). Pyrrolidine has been reported to have catalytic ability for the imine formation.[24] This kind of base catalyst not only maintains the inorganic component within the hybrid body, but also greatly improved the BET surface area of the bulk COF(TpBD) (1883 $m^2 g^{-1}$, Figure S7a), which is close to the theoretical value (2319 $m^2 g^{-1}$, Figure S7b) and far larger than that obtained by the acid-catalysis method (620 $m^2 g^{-1}$, Figure S7a). This unprecedented system is an interesting and competitive alternative to the conventional synthesis of imine-COFs. The study into the aminocatalytic mechanism is currently ongoing.

The two-step method reported herein could prepare the COF-based microspheres not only with uniformity in colloidal size, shape, and structure, but also with flexible controllability in the thickness of COF(TpBD) shell. By varying the monomer concentrations for the polyimine polymerization, the amorphous shell was formed with different thickness. Because of little change in the shell reconstruction, the resulting sizes of COF(TpBD) shells coincided with those of the corresponding polyimine shells. HR-TEM images showed that the rough thickness of COF(TpBD) shell varied from 20 nm, 50 nm to 100 nm by increasing the initial monomer concentrations (Figure 2 a–c), while the particles fused together at the higher concentration under otherwise identical conditions (Figure S8). This is also unparalleled because so far, there has been no method reported for modulation of the grain sizes of nanoCOFs. An insight was made into the evolution of the COF(TpBD) shell. When the structural reconstruction was carried out over 24 h, 48 h, and 72 h, the shell morphology and size were barely changed (Figure S9), but simultaneously, the crystallinity and BET surface areas

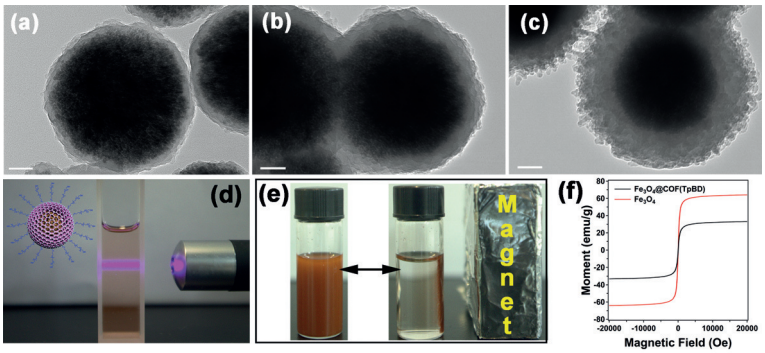

Figure 2. a–c) HR-TEM images of the Fe_3O_4@COF(TpBD) microspheres with the shell thickness of 20 nm (a), 50 nm (b), and 100 nm (c). d,e) Photographs of the dispersion of PEG-grafted Fe_3O_4@COF(TpBD) microspheres in water (d) and their attraction to a magnet (e). f) The magnetic hysteresis curves of Fe_3O_4 and Fe_3O_4@COF(TpBD) microspheres. All of the scale bars in a)–c) are 50 nm. The aqueous solution in (d) was diluted to clearly show the dispersion stability of microspheres, and that in (e) is cloudy because it contains a high concentration of microspheres.

were both largely enhanced as the reaction progressed (Figure S10,S11). The results imply that the crystallization is a process of the internal dynamic imine exchange without addition of more monomers. Analogously, it has been reported that covalent triazine frameworks could be reorganized from their amorphous counterparts under ionothermal conditions.[25]

To modify the surface chemistry of COF-based microspheres for biomedical applications, amine-terminated PEG was allowed to react with the residual aldehyde groups around the edges of the honeycomb-like COF structure, reaching a loading content of 14 wt% (Figure S12). The PEG-modified COF hybrid microspheres exhibited largely improved solution properties (Figure 2d), ensuring their ability to be stable for long-term circulation in body. Also, they could be rapidly attracted to a magnet and re-dispersed in aqueous solution without any remanent magnetism. The saturation magnetization of the composite microspheres was estimated to be as high as 32 emu g^{-1}. Compared with the pure Fe_3O_4 (64 emu g^{-1}), the magnetic content in the COF-based microspheres reached 50%.

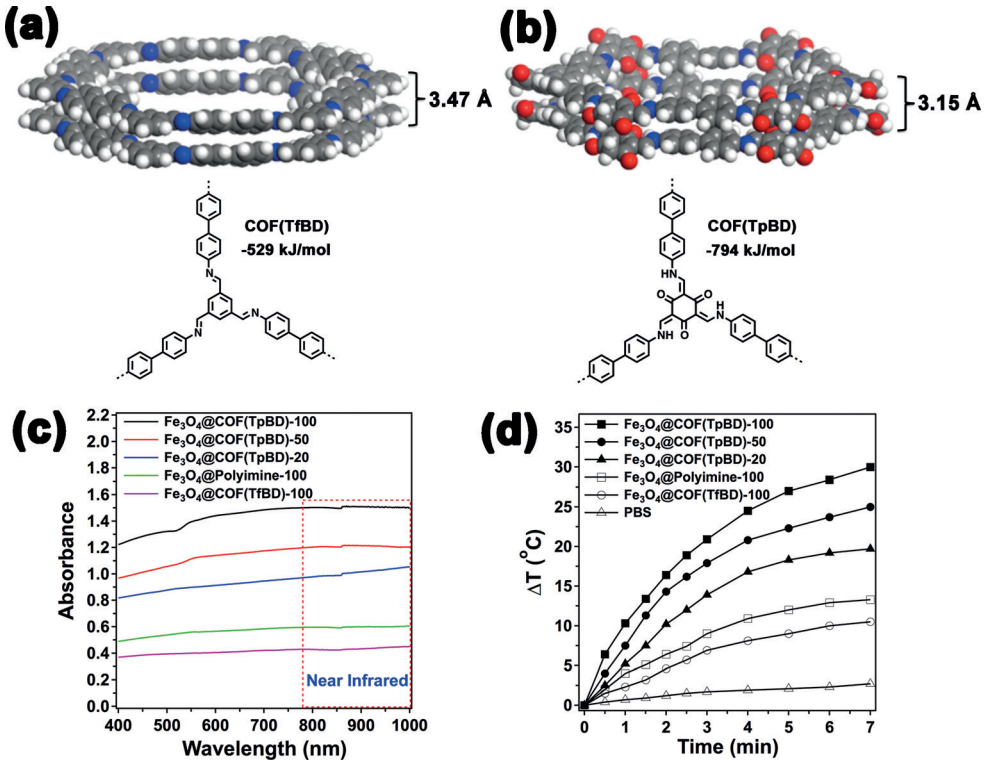

Figure 3. Calculated atomic structures of hexagonal macrocycles of COF (TfBD) (a) and COF(TpBD) (b), which contain different central cores. c) UV/Vis-NIR spectra of core–shell COF composite microspheres dispersed in PBS at a concentration of 200 ppm, with shell thicknesses of 20, 50, and 100 nm. d) Elevated temperature change for the dispersions of different microspheres (200 ppm) and PBS as control upon exposure to 785 nm laser for 7 min at a power density of 5 W cm^{-2}.

It has never been reported whether the imine-COFs have photothermal conversion ability, although they feature a large π-electronic conjugation and strong π–π interaction between the interlayers, both of which might allow them to behave as dipole antennae within broad absorption spectra and release vibrational energy to produce localized heat. We commenced the study on calculating the interlayered packing efficiency of imine-linked COF(TfBD) and COF(TpBD) (Figure 3a,b). It was found that COF(TfBD) had an interlayer distance of 3.47 Å which was considerably larger than that of COF-(TpBD) (3.15 Å). The interlayer distances correspond well with the π–π stacking energy, meaning that the closer packing has the higher stacking energy. As expected, the π–π stacking energy of COF(TpBD) (−794 kJ mol^{-1}) was larger than that of COF(TfBD) (−529 kJ mol^{-1}; see Supporting Information for the detailed calculation). The results imply the fact that the keto forms sitting on the nodes of COF(TpBD) facilitate the intralayer planarity via the NH···O hydrogen bonds and promote the π-electronic conjugation and transportation within the intralayer itself and between the neighboring sheets as well.

The photothermal conversion performance of COF microspheres in water was evaluated for the potential of use in therapeutic applications. Prior to the light irradiation experiments, the optical properties of the aqueous dispersion containing 200 ppm of the hybrid microspheres were examined by using UV/Vis-NIR spectroscopy. As displayed in Figure 3c, all of samples have no evident absorption peak, while exhibit the broad absorption over a wide range from the visible to NIR region. Compared with the microspheres with polyimine shells, the NIR absorbance of COF(TpBD) was largely enhanced due to the well-organized stacking in shell, which also could modulate the absorbance by varying the COF shell thickness. The NIR absorption capability of the Fe_3O_4@COF(TpBD)-100 microspheres was evaluated by calculating the molar extinction coefficient (see Supporting Information for the detailed calculation). The obtained value was as high as 4.2×10^{10} M^{-1} cm^{-1} at 785 nm, which indicates their great potential of photothermal conversion. As shown in Figure 3d, the temperature elevation of the aqueous dispersions containing different microspheres was measured under 785 nm laser irradiation with a powder density of 5 W cm^{-2}. The control experiment indicated that the PBS aqueous solution just showed a little temperature change. With addition of the different microspheres, the system temperature reached a maximum temperature in only 7 min. The temperature change was remarkable on the COF(TpBD)-

based microspheres, and was more significant with increase of the shell thickness. The greatest heat was generated on the Fe_3O_4@COF(TpBD)-100 microspheres (200 ppm), giving a temperature rise of 25 °C, indicating that they could rapidly and efficiently covert the 785 nm laser energy into thermal energy. Also, the photothermal conversion efficiency was measured by the time constant method (Figure S13a,b).[26] Following the Roper's report (See Supporting Information for the detailed calculation), the photothermal conversion efficiency for the Fe_3O_4@COF(TpBD)-100 was calculated to be 21.5 % at 785 nm, about 2–3 times higher than that of the Fe_3O_4 nanoclusters used alone (Figure S13c–f). This is comparable to some of the well-established photosensitizers, such as Au nanoshell (13–25 % at 808 nm),[27a,b,c] Au nanorod (21–50 % at 808 nm),[27a,b,c] $Cu_{2-x}Se$ nanoparticles (22 % at 808 nm),[27c] and Cu_9S_5 nanoplates (25.7 % at 980 nm).[27d] Moreover, for the COFs, there is still room for great improvement because such a 2D organic materials offer a great variety of functionalization through molecular design and reticular polymerization.

In summary, we have developed a general method for the precise construction and functionalization of nanoCOFs by a disorder-to-order dynamic process, which allows for rearrangement of amorphous polyimine networks into crystalline imine-linked COFs without a change of morphology and size. The resulting nanoCOFs are employed to construct a well-defined core–shell nanostructure while retaining crystallinity and periodic micropores, and could be further modulated with a shell of controllable thickness via a template-mediated polymerization and in situ crystallization. The efficient photothermal conversion is found for the Fe_3O_4@COF(TpBD) microspheres, which allows the quick transduction of NIR energy to local heat by strengthening the π-electronic conjugation within the stacking 2D layers. This strategy is general and, in principle, can be used to generate a large pool of COF-based nanomaterials with applicability and functionality that can be deliberately and finely tuned through the design of the organic/inorganic components. Looking forward, this work should also facilitate the coating of COFs onto structurally tailorable supports, opening up a promising pathway for realizing porous organic polymers with applications spanning bio-imaging, phototherapy, and drug delivery.

Acknowledgements

This work is supported by the State Key Project of Research and Development (2016YFC1100300), NSFC (21474015, 51633001) and STCSM (14ZR1402300).

Keywords: composite microspheres · covalent organic frameworks · imines · nanoclusters · photothermal conversion

How to cite: *Angew. Chem. Int. Ed.* **2016**, *55*, 13979–13984
Angew. Chem. **2016**, *128*, 14185–14190

[1] a) F. J. Uribe-Romo, J. R. Hunt, H. Furukawa, C. Klöck, M. O'Keeffe, O. M. Yaghi, *J. Am. Chem. Soc.* **2009**, *131*, 4570–4571; b) M. G. Rabbani, A. K. Sekizkardes, Z. Kahveci, T. E. Reich, R. Ding, H. M. El-Kaderi, *Chem. Eur. J.* **2013**, *19*, 3324–3328.

[2] a) S. Kandambeth, A. Mallick, B. Lukose, M. V. Mane, T. Heine, R. Banerjee, *J. Am. Chem. Soc.* **2012**, *134*, 19524–19527; b) B. P. Biswal, S. Chandra, S. Kandambeth, B. Lukose, T. Heine, R. Banerjee, *J. Am. Chem. Soc.* **2013**, *135*, 5328–5331; c) S. Chandra, S. Kandambeth, B. P. Biswal, B. Lukose, S. M. Kunjir, M. Chaudhary, R. Babarao, T. Heine, R. Banerjee, *J. Am. Chem. Soc.* **2013**, *135*, 17853–17861.

[3] F. J. Uribe-Romo, C. J. Doonan, H. Furukawa, K. Oisaki, O. M. Yaghi, *J. Am. Chem. Soc.* **2011**, *133*, 11478–11481.

[4] a) P. Kuhn, M. Antonietti, A. Thomas, *Angew. Chem. Int. Ed.* **2008**, *47*, 3450–3453; *Angew. Chem.* **2008**, *120*, 3499–3502; b) S. Dalapati, S. Jin, J. Gao, Y. Xu, A. Nagai, D. Jiang, *J. Am. Chem. Soc.* **2013**, *135*, 17310–17313.

[5] C. R. DeBlase, K. E. Silberstein, T.-T. Truong, H. D. Abruña, W. R. Dichtel, *J. Am. Chem. Soc.* **2013**, *135*, 16821–16824.

[6] A. P. Côté, A. I. Benin, N. W. Ockwig, M. O'Keeffe, A. J. Matzger, O. M. Yaghi, *Science* **2005**, *310*, 1166–1170.

[7] a) X. Feng, X. Ding, D. Jiang, *Chem. Soc. Rev.* **2012**, *41*, 6010–6022; b) P. J. Waller, F. Gándara, O. M. Yaghi, *Acc. Chem. Res.* **2015**, *48*, 3053–3063.

[8] a) H. Furukawa, O. M. Yaghi, *J. Am. Chem. Soc.* **2009**, *131*, 8875–8883; b) N. Huang, X. Chen, R. Krishna, D. Jiang, *Angew. Chem. Int. Ed.* **2015**, *54*, 2986–2990; *Angew. Chem.* **2015**, *127*, 3029–3033.

[9] a) S.-Y. Ding, J. Gao, Q. Wang, Y. Zhang, W.-G. Song, C.-Y. Su, W. Wang, *J. Am. Chem. Soc.* **2011**, *133*, 19816–19822; b) H. Xu, J. Gao, D. Jiang, *Nat. Chem.* **2015**, *7*, 905–912.

[10] a) S. Wan, J. Guo, J. Kim, H. Ihee, D. Jiang, *Angew. Chem. Int. Ed.* **2008**, *47*, 8826–8830; *Angew. Chem.* **2008**, *120*, 8958–8962; b) S. Dalapati, E. Jin, M. Addicoat, T. Heine, D. Jiang, *J. Am. Chem. Soc.* **2016**, *138*, 5797–5800; c) G. Lin, H. Ding, D. Yuan, B. Wang, C. Wang, *J. Am. Chem. Soc.* **2016**, *138*, 3302–3305.

[11] S.-Y. Ding, M. Dong, Y.-W. Wang, Y.-T. Chen, H.-Z. Wang, C.-Y. Su, W. Wang, *J. Am. Chem. Soc.* **2016**, *138*, 3031–3037.

[12] S. Chandra, T. Kundu, S. Kandambeth, R. BabaRao, Y. Marathe, S. M. Kunjir, R. Banerjee, *J. Am. Chem. Soc.* **2014**, *136*, 6570–6573.

[13] a) L. Chen, K. Furukawa, J. Gao, A. Nagai, T. Nakamura, Y. Dong, D. Jiang, *J. Am. Chem. Soc.* **2014**, *136*, 9806–9809; b) S. Jin, M. Supur, M. Addicoat, K. Furukawa, L. Chen, T. Nakamura, S. Fukuzumi, S. Irle, D. Jiang, *J. Am. Chem. Soc.* **2015**, *137*, 7817–7827; c) X. Chen, M. Addicoat, E. Jin, L. Zhai, H. Xu, N. Huang, Z. Guo, L. Liu, S. Irle, D. Jiang, *J. Am. Chem. Soc.* **2015**, *137*, 3241–3247.

[14] a) T.-Y. Zhou, F. Lin, Z.-T. Li, X. Zhao, *Macromolecules* **2013**, *46*, 7745–7752; b) S. Kandambeth, V. Venkatesh, D. B. Shinde, S. Kumari, A. Halder, S. Verma, R. Banerjee, *Nat. Commun.* **2015**, *6*, 6786; c) A. Halder, S. Kandambeth, B. P. Biswal, G. Kaur, N. C. Roy, M. Addicoat, J. K. Salunke, S. Banerjee, K. Vanka, T. Heine, S. Verma, R. Banerjee, *Angew. Chem. Int. Ed.* **2016**, *55*, 7806–7810; *Angew. Chem.* **2016**, *128*, 7937–7941.

[15] a) Q. Fang, J. Wang, S. Gu, R. B. Kaspar, Z. Zhuang, J. Zheng, H. Guo, S. Qiu, Y. Yan, *J. Am. Chem. Soc.* **2015**, *137*, 8352–8355; b) L. Bai, S. Z. F. Phua, W. Q. Lim, A. Jana, Z. Luo, H. P. Tham, L. Zhao, Q. Gao, Y. Zhao, *Chem. Commun.* **2016**, *52*, 4128–4131.

[16] S. Lal, S. E. Clare, N. J. Halas, *Acc. Chem. Res.* **2008**, *41*, 1842–1851.

[17] D. Jaque, L. M. Maestro, B. del Rosal, P. Haro-Gonzalez, A. Benayas, J. L. Plaza, E. M. Rodriguez, J. G. Solé, *Nanoscale* **2014**, *6*, 9494–9530.

[18] a) K. Yang, S. Zhang, G. Zhang, X. Sun, S.-T. Lee, Z. Liu, *Nano Lett.* **2010**, *10*, 3318–3323; b) J. T. Robinson, S. M. Tabakman, Y. Y. Liang, H. L. Wang, H. S. Casalongue, D. Vinh, H. J. Dai, *J. Am. Chem. Soc.* **2011**, *133*, 6825–6831.

[19] N. C. Gallego, J. W. Klett, *Carbon* **2003**, *41*, 1461 – 1466.
[20] J. Tan, J. X. Wan, J. Guo, C. C. Wang, *Chem. Commun.* **2015**, *51*, 17394 – 17397.
[21] W. F. Ma, Y. Zhang, L. L. Li, L. J. You, P. Zhang, Y. T. Zhang, J. M. Li, M. Yu, J. Guo, H. J. Lu, C. C. Wang, *ACS Nano* **2012**, *6*, 3179 – 3188.
[22] B. J. Smith, A. C. Overholts, N. Hwang, W. R. Dichtel, *Chem. Commun.* **2016**, *52*, 3690 – 3693.
[23] J. H. Chong, M. Sauer, B. O. Patrick, M. J. MacLachlan, *Org. Lett.* **2003**, *5*, 3823 – 3826.
[24] S. Morales, F. G. Guijarro, J. L. G. Ruano, M. B. Cid, *J. Am. Chem. Soc.* **2014**, *136*, 1082 – 1089.
[25] S. Kuecken, J. Schmidt, L. Zhi, A. Thomas, *J. Mater. Chem. A* **2015**, *3*, 24422 – 24427.
[26] D. K. Roper, W. Ahn, M. Hoepfner, *J. Phys. Chem. C* **2007**, *111*, 3636 – 3641.
[27] a) P. Huang, J. Lin, W. Li, P. Rong, Z. Wang, S. Wang, X. Wang, X. Sun, M. Aronova, G. Niu, R. D. Leapman, Z. Nie, X. Chen, *Angew. Chem. Int. Ed.* **2013**, *52*, 13958 – 13964; *Angew. Chem.* **2013**, *125*, 14208 – 14214; b) V. P. Pattani, J. W. Tunnell, *Lasers Surg. Med.* **2012**, *44*, 675 – 684; c) Q. Tian, F. Jiang, R. Zou, Q. Liu, Z. Chen, M. Zhu, S. Yang, J. Wang, J. Wang, J. Hu, *ACS Nano* **2011**, *5*, 9761 – 9771; d) C. M. Hessel, V. P. Pattani, M. Rasch, M. G. Panthani, B. Koo, J. W. Tunnell, B. A. Korgel, *Nano Lett.* **2011**, *11*, 2560 – 2566.

Received: June 27, 2016
Revised: August 21, 2016
Published online: October 6, 2016

